Journal of Photochemistry, *16* (1981) 147 - 168

MODULATED PHOTOLYSIS OF THE OZONE–WATER VAPOUR SYSTEM: KINETICS OF THE REACTION OF OH WITH HO_2

J. P. BURROWS, R. A. COX and R. G. DERWENT

Environmental and Medical Sciences Division, AERE, Harwell, Oxfordshire OX11 0RA (Gt. Britain)

(Received December 16, 1980; in revised form February 10, 1981)

Summary

The molecular modulation technique was employed to observe the kinetic behaviour of OH and HO_2 radicals in the 253.7 nm photolysis of O_3–H_2O–O_2–N_2 (or O_3–H_2O–O_2–He) mixtures at 1 atm pressure. The radicals were monitored in absorption at 308.2 nm and 210 nm respectively. The rate coefficient for reaction (6) $OH + HO_2 \rightarrow H_2O + O_2$ was determined by computer simulation of the results; the value obtained was $k_6 = (6.2^{+4.0}_{-2.0}) \times 10^{-11}$ cm^3 molecule^{-1} s^{-1} which was independent of temperature in the range 288 - 348 K. The possible role of polyoxide HO_x complexes in reaction (6) is discussed.

1. Introduction

Studies [1 - 5] of the Hartley band photolysis of dilute mixtures of O_3 in the presence of water vapour have shown that the overall decomposition of ozone occurs by a short chain reaction described by the following elementary steps:

	$O_3 + h\nu \rightarrow O(^1D) + O_2$	$k_a[O_3]$	
	$O(^1D) + M \rightarrow O(^3P) + M$	($M \equiv O_2, N_2$ etc.)	(1)
initiation	$O(^1D) + H_2O \rightarrow 2OH$		(2)
chain	$OH + O_3 \rightarrow HO_2 + O_2$		(3)
	$HO_2 + O_3 \rightarrow OH + 2O_2$		(4)
termination	$HO_2 + HO_2 \rightarrow H_2O_2 + O_2$		(5)
	$OH + HO_2 \rightarrow H_2O + O_2$		(6)

Direct measurements of the rate constants of the elementary reactions in isolation lend support to the plausibility of this mechanism.

0047-2670/81/0000-0000/$02.50

This system offers one of the few experimental systems which can provide kinetic information on reaction (6). Relatively high values of the concentration ratio $[OH]/[HO_2]$ can be obtained in steady state photolysis because reaction (3) is slow. This results in a key role for reaction (6) in the termination of the active chain carriers.

When H_2 or CO are present in excess, and when $[O_2]$ is relatively large, OH is rapidly converted to HO_2, *e.g.*

$$OH + H_2 \text{ (or CO)} \rightarrow H + H_2O \text{ (or } CO_2) \quad (7)$$

$$H + O_2 + M \rightarrow HO_2 + M \quad (8)$$

Under these conditions termination by reaction (5) predominates.

There have been a number of studies of the kinetics of reaction (6) since it plays an important role in a variety of laboratory systems as well as in combustion and atmospheric chemistry. Important differences have emerged in the experimentally determined values of k_6. Specifically, studies in flames [6] and at low pressure (1 - 5 Torr) in discharge flow systems [7 - 10] have yielded values of k_6 in the range $(2 - 5) \times 10^{-11}$ cm^3 molecule^{-1} s^{-1} whereas steady state photolysis [5, 6], flash photolysis [11, 12] and pulse radiolysis [13] studies at pressures above 1 atm indicate a high value of $(1 - 2) \times 10^{-10}$ cm^3 molecule^{-1} s^{-1}. Clearly more measurements of k_6 under a variety of different conditions may help to resolve this problem.

In the present work the 253.7 nm photolysis of O_3–H_2O–O_2 mixtures was investigated using molecular modulation spectrometry to monitor directly the concentration and lifetime of both OH and HO_2 radicals. O_3 concentrations were also monitored, using conventional absorption spectrometry, to obtain overall O_3 decay quantum yields. The kinetic parameters were obtained by computer simulation.

2. Experimental

The experiments were conducted in the molecular modulation apparatus described previously [14]. The silica reaction cell (86 cm long) was irradiated with up to six low pressure mercury lamps emitting radiation primarily near 253.7 nm (Philips TUV 30 W); the radiation was modulated with a square wave at frequencies between 0.3 and 50 Hz. HO_2 absorption was monitored at 210 nm using light from a stabilized deuterium lamp (Manufacturers Supply Ltd.) which was resolved on a 0.25 m double monochromator (Spex Doublemate) with a spectral slit width of 3 nm. OH was measured by resonance absorption of radiation emitted from a microwave-powered discharge lamp through which moist argon flowed at 1 Torr pressure. The monitoring beam was dispersed in a 0.75 m monochromator (Spex model 1700) with a spectral slit width of 0.1 nm centred on 308.2 nm, the maximum of the Q_{13} line in the $\tilde{A}\ ^2\Sigma^+ - \tilde{X}\ ^2\Pi$ system of OH. The modulated absorption was detected on a photomultiplier and was fed to a digital lock-in system which provided separate in-phase and in-quadrature components of absorption, P and Q respectively. The minimum detectable modulated absorption was about

2×10^{-5}, corresponding to concentrations of approximately 5×10^{10} molecules cm^{-3} and 2×10^{9} molecules cm^{-3} for HO_2 and OH respectively. O_3 concentration measurements were obtained from absorption measurements at 240 nm.

Reaction mixtures containing O_3 ($(0.4 - 4) \times 10^{15}$ molecules cm^{-3}) and H_2O ($(1 - 5) \times 10^{17}$ molecules cm^{-3}) diluted in O_2–N_2 or O_2–He at a total pressure of 1 atm flowed through the cell with a residence time of 15 - 45 s. Measurements of radical absorption were made on the flowing mixture under modulated photolysis after steady conditions had been attained. Typically about 30% of the O_3 was decomposed in the cell. Since O_3 has a significant absorption cross section (5.0×10^{-19} cm^2 [15]) at 210 nm (the monitoring wavelength for HO_2), the O_3 concentration changes in the cell gave rise to additional modulated absorption which appeared mainly as an in-quadrature component at low frequency. A correction was made to the observed value of Q on the assumption that O_3 consumption occurred only during photolysis; this led to a "saw-tooth" waveform with an in-quadrature amplitude component of $\Delta V\tau/8$, where ΔV is the voltage change per cycle and τ is the modulation period. Since the radical species which react with O_3 have a finite lifetime, this assumption is not strictly true for all modulation periods. The errors introduced were subsequently explored in computer simulations of the experiments and were found to be small but significant. The O_3 absorption at 308.2 nm was too weak to influence the measurements of OH absorption.

O_3 decay quantum yields were determined from measurements of O_3 decay in a static system. Experiments with excess H_2 present were also conducted in a static system and a correction for the O_3 absorption at 210 nm on the HO_2 signals was made as described previously [16] for this type of experiment. All processing of the signals from the digital lock-in system was performed on-line using a small computer (Commodore PET 3200), and radical absorption components were printed out together with other experimental parameters.

O_2 (breathing grade BOC) was purified by passage over CuO at 633 K, soda lime and an activated molecular sieve. CH_4 at 16 - 18 ppm remained as the only detectable hydrogenous impurity. The amount of CO was less than 0.1 ppm. O_3 was produced in the O_2 stream either by UV irradiation (using Philips OZ4 lamps) or, when higher O_3:O_2 concentration ratios were required, by passage through a small silent discharge ozonizer. The O_2–O_3 flow was then mixed with a stream of nitrogen or helium, part of which was saturated with water vapour to provide the required composition. Experiments were conducted at 288, 308 and 348 K.

3. Results

3.1. Photolysis of H_2–O_3–O_2 mixtures: determination of the O_3 photolysis rate

Mixtures of H_2, O_2 and O_3 (1.7×10^{19} molecules cm^{-3}, 0.6×10^{19} molecules cm^{-3} and 7×10^{14} molecules cm^{-3} respectively) were photolysed

and the HO_2 absorption was measured over a range of modulation frequencies from 0.3 to 25 Hz. In this system $O(^1D)$ reacts predominantly with H_2:

$$O(^1D) + H_2 \rightarrow H + OH \quad (9)$$

The fraction f' of $O(^1D)$ reacting by reaction (9) was 0.90 - 0.95, and the subsequent chemistry is dominated by reactions (7), (8) and (5). The kinetic behaviour of HO_2 is described by

$$\frac{d[HO_2]}{dt} = 2B - 2k_5[HO_2]^2 \quad (I)$$

Here $2B$ is the total production rate of HO_2 when the lights are on and is equal to $2f'k_a[O_3]$, where k_a is the rate of photolysis of O_3 to give $O(^1D)$. In the dark $B = 0$. The solution of the second-order kinetic equation (I) for the square-wave-modulated system has been described previously [14]. The measured parameters P and Q are functions of B, k_5 and the HO_2 absorption cross section σ_{HO_2} at the monitoring wavelength. Since the cross section is known (4.3×10^{-18} cm^2 at 210 nm [16]), B and k_5 can be evaluated.

Figure 1 shows data for P and Q as functions of τ for different photolytic intensities. The form of the curves is typical of a photochemically modulated transient species, with large in-phase absorption at low frequency when the radical concentration oscillates between a low value in the dark and its steady state during illumination. As the photolysis period decreases and becomes comparable with the radical lifetime, an increasing proportion

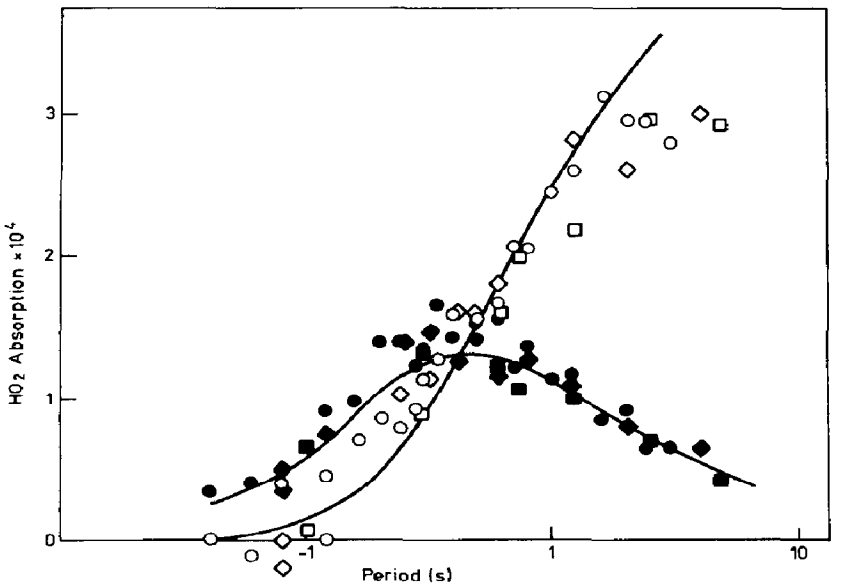

Fig. 1. In-phase (○, □, ◇) and in-quadrature (●, ■, ◆) absorption of HO_2 at 210 nm in the photolysis of O_3–O_2–H_2 mixtures at 308 K: ○, ●, one-lamp photolysis; ◇, ◆, four-lamp photolysis; □, ■, six-lamp photolysis. The data were normalized as described in the text. The curves show best-fit second-order curves using $k_5 = 2.08 \times 10^{-12}$ cm^3 molecule^{-1} s^{-1} ($HO_2 + HO_2 \rightarrow H_2O_2 + O_2$).

of the absorption appears in the in-quadrature component and the overall magnitude of the modulation decreases.

The data in Fig. 1 were normalized by dividing the absorption components and multiplying the period by $n^{1/2}$ (n is the number of photolysis lamps). For second-order kinetics the normalized absorption components as functions of τ should then be represented by a single pair of curves. A pair of second-order curves generated by a weighted least-squares fitting method are seen to describe the data well, except the in-phase absorption at low frequency where the large correction, due to O_3 absorption, may be a source of error. These curves correspond to $k_5 = 2.08 \times 10^{-12}$ cm^3 molecule^{-1} s^{-1}, $k_a = 2.4 \times 10^{-2}$ s^{-1} lamp^{-1}.

The average values of k_5 and k_a from experiments at 308 and 348 K with and without H_2O present are summarized in Table 1. The value of k_a decreased with an increase in temperature owing to a decrease in the lamp output at elevated temperatures. The values of k_5 agree closely with those obtained previously [16] and confirm the negative temperature coefficient for this reaction. The presence of H_2O caused a slight increase in k_5 at both temperatures but the increase was not significant.

3.2. *The photolysis of O_3–O_2–H_2O–N_2 mixtures*

In these experiments concentrations of O_2–N_2 were typically in 100-fold excess over the concentration of H_2O and the predominant fate of $O(^1D)$ was deactivation to $O(^3P)$ by reaction (1) with the subsequent formation of O_3 by

$$O(^3P) + O_2 + M \rightarrow O_3 + M \qquad (10)$$

which is the only important reaction of $O(^3P)$ for all the experimental conditions used here. The fraction f of $O(^1D)$ reacting with H_2O was 0.03 - 0.10, as calculated from the relative rate coefficients for $O(^1D)$ reactions given in the recent CODATA evaluation [17]. The overall effect is a net production of HO_x species and consequent O_3 decay, involving reactions (3) - (6). Measurements of the modulated absorption components of HO_2 and OH as functions of τ were made at different radical production rates B obtained by varying f (using different $[H_2O]$), k_a (using different photolysis intensities) and $[O_3]$.

TABLE 1

Values of k_a and k_5 obtained from photolysis of H_2–O_2–O_3 mixtures

Temperature (K)	P_{H_2O} (Torr)	$k_a \times 10^2$ (s^{-1} lamp^{-1})	$k_5 \times 10^{12}$ (cm^3 molecule^{-1} s^{-1})
308	0	2.44 ± 0.10	2.08 ± 0.20
	3.0	2.43 ± 0.20	2.20 ± 0.20
348	0	1.75 ± 0.30	1.34 ± 0.15
	10.5	1.67 ± 0.27	1.58 ± 0.15

The error limits of $\pm 2\sigma$ were obtained from the fitting procedure.

A typical set of data illustrating the dependences of P and Q on τ for HO_2 at 308 K are shown in Fig. 2. The form of the curves is again typical of a transient species. From such curves the period τ_0 corresponding to the point where $P = Q$ and the magnitude A_{τ_0} of the absorption at this point could be determined. These quantities are a measure of the lifetime of HO_2 and the concentration modulation of HO_2 respectively and are related to the rate parameters of the elementary reactions controlling HO_2 kinetics. However, because of the complexity of the chemistry a simple analytical derivation of the relationships was not possible and computer simulation and fitting techniques were used to obtain rate constants from the data.

The effect of experimental variables on τ_0^{-1} and A_{τ_0} is shown in Fig. 3 in which these parameters are plotted against $(fk_a[O]_3)^{1/2}$, *i.e.* $B^{1/2}$, where B is one-half of the total production rate of OH radicals when the lights are on. The purpose of this plot is to explore possible pseudo-second-order kinetic behaviour of HO_2, which is expected in a chain reaction system where the chain carrier radicals are initiated and terminated in pairs. There is some scatter due partly to the random errors in the measurements of the rather small absorptions but there is nevertheless an indication of an approximately linear relationship between the kinetically significant parameters and the square root function over the experimental range. The curves indicate trends obtained by computer simulation and are discussed later. A significant effect of temperature on the τ_0 and A_{τ_0} values is evident from Fig. 3. The lifetime parameter τ_0^{-1} at a given value of $B^{1/2}$ shows a tendency to increase with decreasing temperature whilst the A_{τ_0} parameter exhibits a trend in the reverse direction.

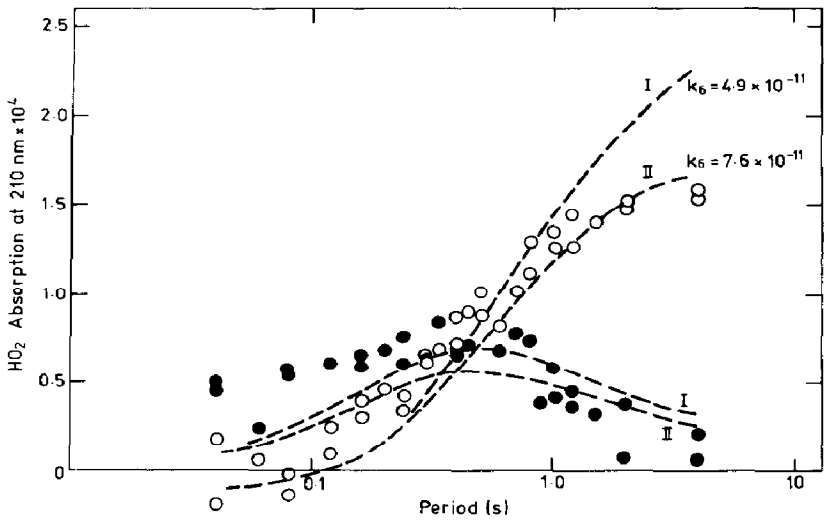

Fig. 2. In-phase (○) and in-quadrature (●) absorption of HO_2 at 210 nm as functions of the photolysis period τ in the six-lamp photolysis of O_3 (2.38×10^{15} molecules cm^{-3}) in the presence of H_2O (1.38×10^{17} molecules cm^{-3}) and O_2–N_2 (1:1 mole ratio) at 1 atm pressure and 308 K: – – –, computer fits to experimental data using equal weight to all data points (I) and points weighted by τ/τ_0 or τ_0/τ where τ is the period corresponding to the curve crossing (II). The corresponding "best-fit" values of k_6 are indicated.

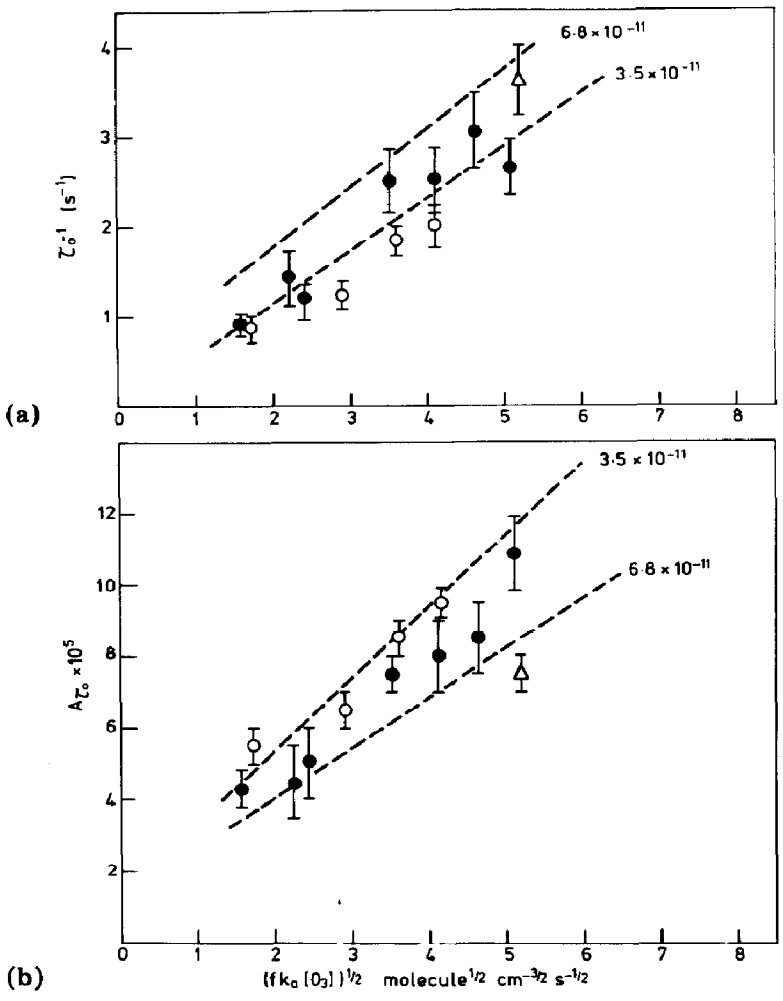

Fig. 3. Plots of (a) the inverse of the period τ_0 and (b) the modulated absorption A_{τ_0} of HO_2 at 210 nm, the crossing of the in-phase and in-quadrature curves, against the quantity $(fk_a[O_3])^{1/2}$ (see text): △, 288 K; ●, 308 K; ○, 348 K; experimental errors are indicated by error bars; – – –, approximate loci of the dependence of these parameters at 308 K generated in computer simulations using the indicated values of k_6 in units of cubic centimetres per molecule per second.

Figure 4 shows a typical set of OH absorption data plotted against τ. Clearly the lifetime of OH is much shorter than that of HO_2 with the curve-crossing region lying near the limit of the accessible frequency of the experimental system. At $\tau > 0.5$ s P is maximized and Q is nearly zero, *i.e.* the OH concentration–time profile is a square wave in-phase with the photolysis lamps. Under these conditions P is a measure of the steady state concentration of OH achieved when the lights are on:

$$P(\tau > 0.5) = \tfrac{1}{2}\sigma_{OH} l [OH]_{ss}$$

where l is the path length and σ_{OH} is the absorption cross section for OH.

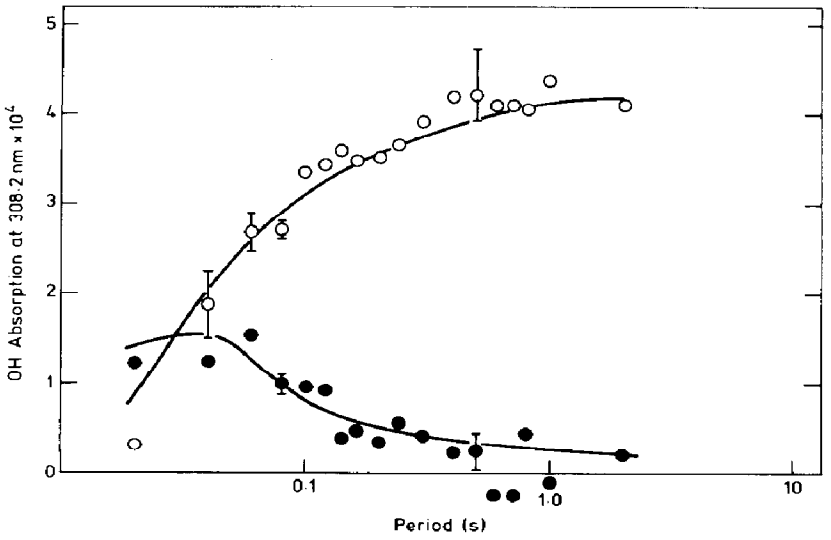

Fig. 4. In-phase (○) and in-quadrature (●) absorption of OH at 308.2 nm in the six-lamp photolysis of O_3 (2.4×10^{15} molecules cm^{-3}) in the presence of H_2O (2.1×10^{17} molecules cm^{-3}) and O_2–N_2 (1:1 mole ratio) at 1 atm pressure and 308 K: ——, computer fits with $k_6 = 2.4^{+2.0}_{-1.0} \times 10^{-11}$ cm^3 $molecule^{-1}$ s^{-1} and $\sigma_{OH} = (7.6 \pm 0.5) \times 10^{-17}$ cm^2; error bars, maximum spread of experimental points.

Figure 5 shows a logarithmic plot of the steady state modulated absorption of OH as a function of the quantity fk_a. It can be seen that the data for O_2–N_2 as diluent are reasonably well defined by a line with a slope of unity, indicating a nearly linear relationship between the variables. The [OH] steady state, however, showed little or no dependence on $[O_3]$ as can be seen by a comparison of the data represented as circles ($[O_3]$ in the range $(1.5 - 2.5) \times 10^{15}$ molecules cm^{-3}) and as triangles ($[O_3]$ in the range $(0.3 - 0.7) \times 10^{15}$ molecules cm^{-3}). In contrast, it was found that the OH lifetime parameter τ_0^{-1} increased markedly with $[O_3]$ but showed little dependence on fk_a, as illustrated in Fig. 6. Changes in $[O_3]$ influence not only the rate of photochemical production of OH but also the rates of OH and HO_2 interconversion by reactions (3) and (4). These results indicate that the OH concentration and lifetime are influenced markedly by the rate of reaction (3). Trends obtained by computer simulations are indicated by the broken curve and are discussed later.

3.3. The photolysis of O_3–O_2–H_2O–He mixtures

In these experiments the O_2 and H_2O concentrations were typically 1×10^{17} molecules cm^{-3} and 2×10^{17} molecules cm^{-3} respectively, with the helium diluent at 1 atm pressure. Since helium does not deactivate $O(^1D)$ to a significant extent [18], the fraction of $O(^1D)$ reacting with H_2O was relatively high, $f = 0.86 - 0.96$. The rate of photolytic production of HO_x species was consequently increased by up to a factor of 30 over that in the experi-

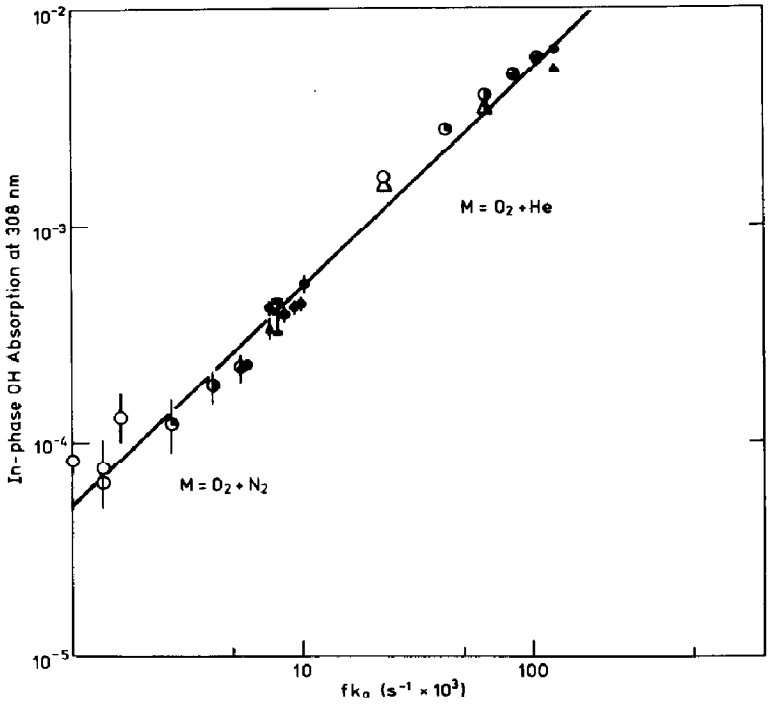

Fig. 5. A logarithmic plot of limiting low frequency in-phase absorption of OH at 308.2 nm against the quantity fk_a (see text) (data in the separate regions were obtained with the different diluent gases as indicated): ▲, ●, six lamps; △, ○, one lamp; ◔, two lamps; ◑, three lamps; ◕, four lamps; ●, five lamps; ○, ◔, ◑, ◕, ●, ●, $[O_3]$ in the range (1.5 - 2.5) × 10^{15} molecules cm^{-3}; △, ▲, $[O_3]$ in the range (0.3 - 0.7) × 10^{15} molecules cm^{-3}; I, change in computed OH absorption with k_6 varied from 2 × 10^{-11} to 25 × 10^{-11} cm^3 molecule^{-1} s^{-1} and σ_{OH} = 9 × 10^{-17} cm^2; |, experimental error.

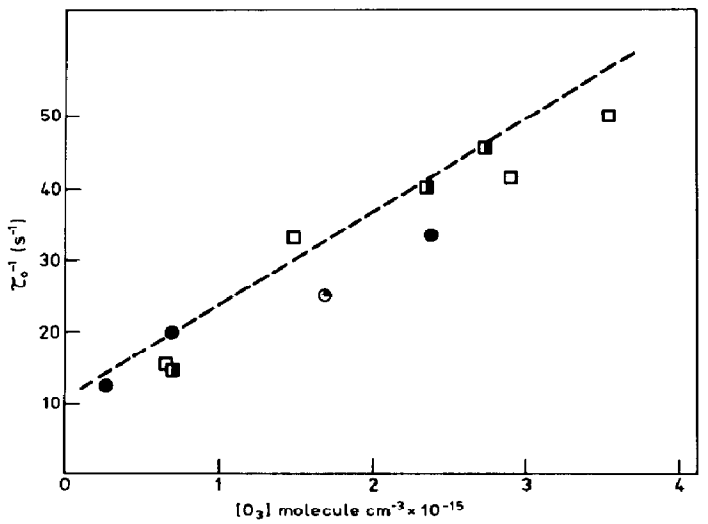

Fig. 6. A plot of τ_0^{-1} from OH absorptions at 308.2 nm against $[O_3]$: ●, ◔, diluent gas, O_2–N_2; □, ◨, diluent gas, helium; ●, six lamps; ◔, ◨, three lamps; □, one lamp; – – –, approximate locus of computed functional dependence.

ments with O_2–N_2 diluent. As before, modulated absorption measurements for HO_2 and OH were made over a range of photochemical production rates.

Figure 7 illustrates typical data for HO_2 absorption as a function of τ using one- and three-lamp photolysis. The threefold change in light intensity had only a small effect on the absorption components and hence on the HO_2 concentration modulation; the magnitude of the absorption was only slightly greater than in the O_2–N_2 diluent (*cf.* Fig. 2) despite the large increase in the HO_x production rate. However, the quantity A_{τ_0} showed a marked dependence on O_3 concentration as can be seen from a plot of these parameters (Fig. 8). It is concluded, therefore, that the behaviour of HO_2 in the O_3–H_2O system changed significantly when the O_2–N_2 diluent was replaced by helium with the consequent large increase in HO_x production.

Figure 9 shows absorption data for OH as a function of τ for one- and three-lamp photolysis. The steady state concentrations of OH were about a factor of 10 higher than in the presence of the O_2–N_2 diluent, allowing precise measurement of its kinetic behaviour. It can be seen from Figs. 5 and 6 that the kinetic behaviour of OH as reflected in the functional plots is similar to that observed in the O_2–N_2 diluent.

3.4. *Measurements of O_3 decay quantum yields $\Phi(-O_3)$*

$\Phi(-O_3)$ was obtained from a comparison of the average rate of O_3 decay over the first 30 s of reaction with the light absorption parameter $B/2$

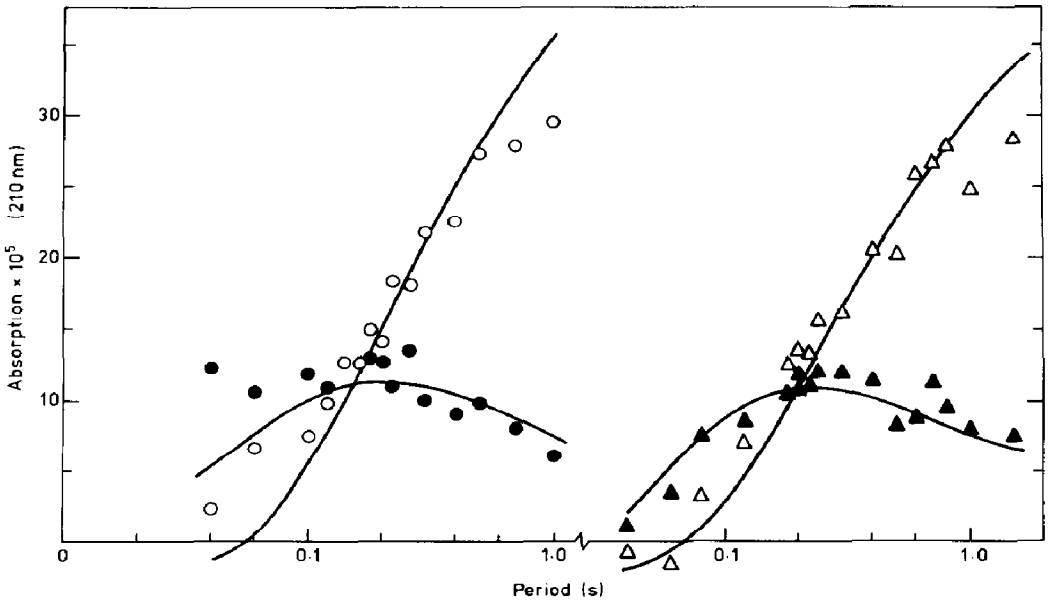

Fig. 7. In-phase (○, △) and in-quadrature (●, ▲) absorption of HO_2 at 210 nm as functions of the photolysis period in the photolysis of O_3 (2.5×10^{15} molecules cm^{-3}) in the presence of H_2O (2.1×10^{17} molecules cm^{-3}) and helium at 1 atm pressure and 308 K: left-hand side, ○, ●, three-lamp photolysis; ——, computed curve for $k_6 = (5.5 \pm 0.6) \times 10^{-11}$ cm^3 $molecule^{-1}$ s^{-1}; right-hand side, △, ▲, one-lamp photolysis; ——, computed curve for $k_6 = (6.3 \pm 0.5) \times 10^{-11}$ cm^3 $molecule^{-1}$ s^{-1}.

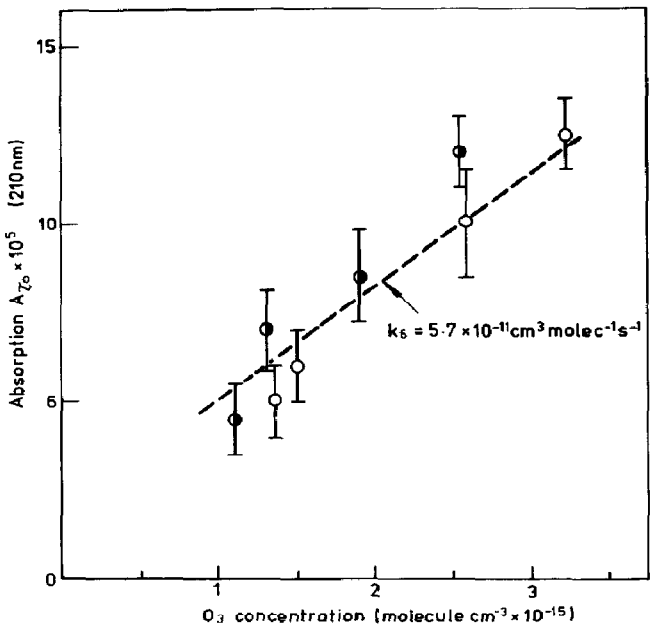

Fig. 8. A plot of HO_2 absorption at the intersection of curves for in-phase and in-quadrature absorption against $[O_3]$ in the photolysis of O_3–H_2O–He mixtures at 308 K: ○, one lamp; ●, three lamps; – – –, approximate locus of computed dependence for k_6 = 5.7×10^{-11} cm^3 molecule^{-1} s^{-1}, the mean value obtained from these data.

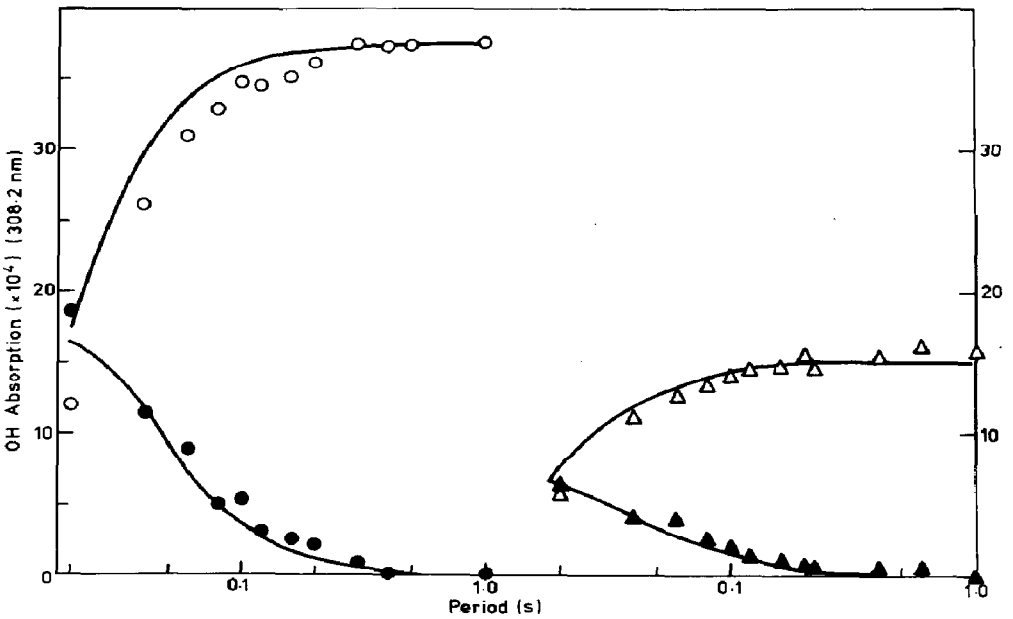

Fig. 9. In-phase (○, △) and in-quadrature (●, ▲) absorption of OH at 308.2 nm as functions of the period τ in the photolysis of O_3–H_2O–He mixtures at 1 atm pressure and 308 K ($[O_3]$, 2.5×10^{15} molecules cm^{-3}; $[H_2O]$, 2.1×10^{17} molecules cm^{-3}): left-hand side, ○, ●, three-lamp photolysis; ——, computed curve for $k_6 = (5.5 \pm 0.6) \times 10^{-11}$ cm^3 molecule^{-1} s^{-1}; $\sigma_{OH} = (1.13 \pm 0.03) \times 10^{-16}$ cm^2; right-hand side, △, ▲, one-lamp photolysis; ——, computed curve for $k_6 = (6.3 \pm 0.5) \times 10^{-11}$ cm^3 molecule^{-1} s^{-1}; $\sigma_{OH} = (1.02 \pm 0.05) \times 10^{-16}$ cm^2.

over this period. A fixed photolysis frequency of 1 Hz was used for these experiments since it was found that there was a small but significant increase in $\Phi(-O_3)$ with increasing frequency. The data for a wide range of B are plotted in Fig. 10 in the form $\Phi(-O_3) - 1$ *versus* $[O_3]/B^{1/2}$. The basis of this plot is a steady state analysis similar to that described by DeMore [5] for the H_2–O_3–O_2 system; a linear relationship is expected for unmodulated photolysis. Although the present data exhibit considerable scatter, they are not well described by a line through the origin. However, the steady state analysis is invalid for modulated photolysis and consequently computer simulation was again used to generate the expected form of the relationship for the present system. The results are described in the following section.

3.5. Determination of k_6

3.5.1. Steady state analysis

The differential equations governing the kinetics of HO_2 and OH in the O_3–H_2O system involving reactions (1) - (6) are

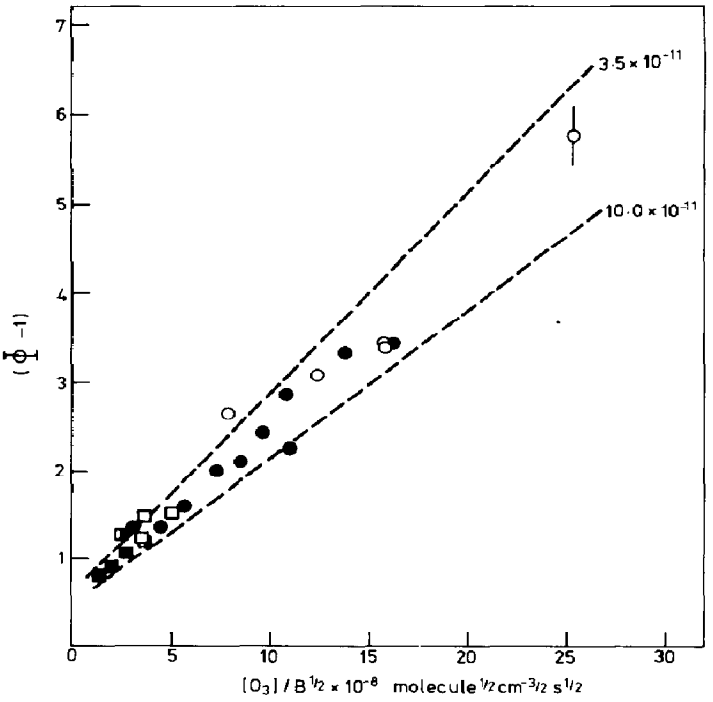

Fig. 10. A plot of $\Phi - 1$ *vs.* $[O_3]/B^{1/2}$ for modulated photolysis (τ = 1 s) of O_3 in the presence of H_2O, where Φ is the quantum yield for O_3 removal (= $d[O_3]/dt$ divided by $\frac{1}{2}fk_a[O_3]$) and $B = \frac{1}{2}fk_a[O_3]$: ○, ●, diluent, O_2–N_2; □, ■, ◨, diluent, helium; ●, ■, six lamps; ◨, three lamps; ○, □, one lamp; – – –, approximate loci of computed functional dependence using indicated values of k_6 in units of cubic centimetres per molecule per second.

$$\frac{d[OH]}{dt} = 2B + k_4[O_3][HO_2] - k_3[OH][O_3] - k_6[OH][HO_2] \quad \text{(II)}$$

$$\frac{d[HO_2]}{dt} = k_3[O_3][OH] - k_4[O_3][HO_2] - 2k_5[HO_2]^2 - k_6[HO_2][OH] \quad \text{(III)}$$

Solution of these equations for the steady state can be obtained for the following limiting conditions.

(1) When $R_3 = R_4 \gg R_5 + R_6$ (R is the reaction rate), *i.e.* for a long chain length, we obtain the relationship $[OH] = (k_4/k_3)[HO_2]$.

Solution of eqns. (II) and (III) then gives

$$[HO_2]_{ss} = \left(\frac{B}{k_5 + k_6k_4/k_3}\right)^{1/2} \quad \text{(IV)}$$

It follows that the concentration modulation of HO_2 and OH should be proportional to $(fk_a[O_3])^{1/2}$.

(2) When $R_6 = R_3 \gg R_4 + R_5$, *i.e.* when all HO_2 radicals are removed by reaction with OH, then

$$[HO_2]_{ss} = \frac{k_3[O_3]}{k_6} \quad \text{(V)}$$

$$[OH]_{ss} = \frac{fk_a}{k_3} \quad \text{(VI)}$$

It is clear from both the quantum yield measurements and the functional plots of HO_2 and OH modulation (Figs. 3 and 5) that the long chain length approximation is not strictly applicable under the present experimental conditions. The approximately linear dependence of HO_2 absorption at τ_0 on $[O_3]$ in the helium diluent experiments (Fig. 8) indicates that $[HO_2]_{ss}$ may be approximated by eqn. (V) under these conditions. Unfortunately the steady state absorption of HO_2 could not be determined from the data, since the limiting low frequency value of P was not approached. A lower limit of $[HO_2]_{ss}$ could be determined from the absorptions observed at $\tau = 1 - 2$ s, which were a factor of 2.7 ± 0.2 greater than A_{τ_0}. Using the known value of σ_{HO_2} a lower limit of $(6.2 \pm 1.1) \times 10^{-4}$ is obtained for the ratio k_3/k_6 from eqn. (V). Use of a consensus value for k_3 of 7.2×10^{-14} cm^3 molecule^{-1} s^{-1} [17] gives

$$k_6 \leqslant (1.2 \pm 0.2) \times 10^{-10} \text{ cm}^3 \text{ molecule}^{-1} \text{ s}^{-1}$$

Although the functional dependence of OH (Fig. 5) is approximately consistent with eqn. (VI) over the experimental range, the data provide no information on the value of k_6. They can be used to obtain an estimate of the absorption cross section of OH for the resonance radiation, *i.e.*

$$\sigma_{OH} = \frac{P_\infty(OH)}{fk_a}\frac{2k_3}{l} \approx 9 \times 10^{-17} \text{ cm}^3 \text{ molecule}^{-1} \text{ s}^{-1}$$

In view of the approximation made, these estimates may be subject to considerable error. Further quantitative analysis was performed using numerical simulation techniques.

3.5.2. Computer analysis

The computer simulations of the results for the determination of k_6 were carried out with the Harwell program FACSIMILE [19] which was used to perform a double integration to obtain experimentally observed variables as functions of the kinetic parameters. Integration of the differential equations describing the time dependence of the chemistry was followed by a second integration through the photolysis cycle to obtain P and Q at a given value of τ. Since the experimental values of P and Q for OH and HO_2 were average values over the length of the reaction cell, the mixture composition was set initially at the mean composition present in the cell with photolysis under steady state flow conditions. In the simulations the concentrations of O_2, N_2 and H_2O were held constant but the O_3 concentration modulation about its mean value was reproduced by the introduction of a time-independent O_3 production term, equal to $\Phi(-O_3)B/2$, which balanced the photochemical removal of O_3. This allowed the modulated absorption components due to O_3 to be computed.

A fitting routine was also incorporated which optimized selected kinetic parameters to minimize the sum of the squares of the deviations between observed and calculated values of P and Q. Simulations for different values of τ, necessary to build up kinetic curves such as those shown in Figs. 1, 2 and 5, were performed simultaneously using FACSIMILE by describing the variables, concentration and absorption as vectors rather than as scalars. For example, instead of performing 10 integrations one after the other to cover a range of frequencies, the variables were made vectors of length 10, each representing a single frequency. Further synchronization of the calculation to reduce the number of operations was achieved by scaling the time in each experiment by the modulation frequency or some multiple of it. Under these conditions concentration modulation waveforms for different frequencies are all generated simultaneously and not sequentially. These techniques reduced computation time sufficiently to allow repeated integrations to be performed as required by the optimization routine and at a reasonable cost in computer time (2 min CPU time on the IBM 3033 computer).

The complete reaction scheme included in the simulations is given in Table 2. Reactions (13) and (14) involving H_2O_2 and also reactions (12) and (15) played only a very minor role but were included for completeness. The reaction of $O(^3P)$ with HO_2 played an insignificant role and was therefore omitted. Photolysis of O_3 at 245 nm produces $O_2(^1\Delta)$ and $O(^1D)$ which generates $O_2(^1\Sigma)$ in the system when it is quenched by O_2. On the basis of available rate coefficient data, the excited states of O_2 do not affect the behaviour of HO_2 or OH nor do they lead to a significant effect on $\Phi(-O_3)$. The reaction of $O_2(^1\Delta)$ or $O_2(^1\Sigma)$ with O_3 does occur but the $O(^3P)$ produced rapidly re-forms O_3 via reaction (10). The rate coefficients in Table 2 were

TABLE 2

Reaction mechanism for O_3–H_2O photolysis

Reaction				k^a
(a)	$O_3 + h\nu$	→ $O(^1D) + O_2(^1\Delta)$		$k_a = 2.38 \times 10^{-2}$ (s^{-1} $lamp^{-1}$)
(1)	$O(^1D) + M$	→ $O(^3P) + M$	($M \equiv O_2, N_2$)	$k_1 = 4.6 \times 10^{-11}$
(2)	$O(^1D) + H_2O$	→ $2OH(^2\Pi)$		$k_2 = 2.8 \times 10^{-10}$
(3)	$OH + O_3$	→ $HO_2 + O_2$		$k_3 = 7.25 \times 10^{-14}$
(4)	$HO_2 + O_3$	→ $OH + 2O_2$		$k_4 = 2.0 \times 10^{-15}$
(5)	$HO_2 + HO_2$	→ $H_2O_2 + O_2$		k_5 (see text)
(6)	$OH + HO_2$	→ $H_2O + O_2$		k_6 (see text)
(10)	$O(^3P) + O_2 + M$	→ $O_3 + M$	($M \equiv O_2, N_2$)	k_{10} [M] = 1.29×10^{-14}
			($M \equiv He$)	k_{10} [M] = 0.76×10^{-14}
(11)	$OH + OH + M$	→ $H_2O_2 + M$	($M \equiv O_2, N_2$)	k_{11} [M] = 14.5×10^{-12}
			($M \equiv He$)	k_{11} [M] = 7.5×10^{-12}
(12)	$OH + OH$	→ $H_2O + O$		$k_{12} = 1.8 \times 10^{-12}$
(13)	$OH + H_2O_2$	→ $HO_2 + H_2O$		$k_{13} = 1.6 \times 10^{-12}$
(14)	$H_2O_2 + h\nu$	→ $2OH(^2\Pi)$		$k_{14} = (6.3 \times 10^{-3})k_a$ (s^{-1})
(15)	OH	→ wall		$k_{15} = 3.0$ (s^{-1})

[a] k is given in units of cubic centimetres per molecule per second unless indicated otherwise; temperature, 300 K; for three-body reactions k[M] is given for [M] = 1 atm pressure.

all taken from the CODATA evaluations [17] with the exceptions of k_5, for which the experimental values determined in this study in the presence of H_2O were used, and k_6, which was varied in the optimization routine to fit the results. The experimental data were averaged to provide pairs of P and Q values at 10 different periods and these were entered with an appropriate weighting factor. When OH absorption data were entered, σ_{OH} was also allowed to float to obtain a best-fit value.

Let us consider first the results of the simulations of the HO_2 data shown in Fig. 2 for the O_2–N_2 diluent. When all the data points were equally weighted with a standard error of 2×10^{-5} units of absorption, the best-fit value of $k_6 = (7.6 \pm 0.9) \times 10^{-11}$ cm^3 $molecule^{-1}$ s^{-1} was obtained. The error limits are the 95% confidence limits estimated by the fitting procedure, making no allowance for any systematic errors. The corresponding curves are seen to give a good fit to the data at low frequency but a poor fit in the curve-crossing region. Experimentally the curve-crossing region is optimum for signal measurement and so this inconsistency is considered to be significant. When optimization was performed with data weighted according to τ_0/τ (or τ/τ_0 for $\tau < \tau_0$) a best-fit value of 4.9×10^{-11} cm^3 $molecule^{-1}$ s^{-1} was obtained. The resulting curves fit the curve-crossing region moderately well but severely overestimate the low frequency absorptions. Both curves satisfy the criteria of a good fit inasmuch as the sum of the squares of the residuals is within the range expected for the weighting factors applied. Neither of the curves shows a good fit to the high frequency data.

Optimized curves for HO_2 data with helium as the diluent gas, uniformly weighted with a standard error of 2×10^{-5}, are shown in Fig. 7. The best-fit

values of k_6 given in Fig. 7 for three- and one-lamp data were intermediate between the two values in Fig. 2 and were in good agreement with each other. It can be seen from Fig. 7 that there is still a tendency for the model to overestimate the low frequency absorption. The OH data were also included in these optimization runs and the corresponding curves are shown in Fig. 9. The fit is excellent except at the very high frequencies where experimental precision is poor, particularly at $\tau = 0.02$ s (50 Hz). The best-fit value of σ_{OH} is well defined and will be discussed later.

When optimization was performed on OH data alone, either the values of k_6 were indeterminate or the solution gave wide confidence limits. It was clear that under the conditions of our experiments the kinetic behaviour of OH was insensitive to the value of k_6. This is illustrated in Fig. 5 where the thick vertical bar indicates the effect of varying k_6 from 2×10^{-11} to 25×10^{-11} cm^3 molecule^{-1} s^{-1} on the OH absorption calculated using $\sigma = 9 \times 10^{-17}$ cm^2. τ_0(OH) also exhibited a very weak dependence on k_6, but the effect of varying [O_3] on τ_0^{-1}(OH) predicted by the computer simulations agreed well with experiment as can be seen from Fig. 6.

Table 3 shows a summary of the values of k_6 and σ_{OH} obtained in the optimization runs which were conducted with uniform weighting of the data points. The average value of k_6 from the helium results was slightly lower than that from the O_2 results, which also showed more spread. The problem of the unsatisfactory fit to both the low frequency and mid-frequency absorption data for HO_2 was also apparent in most of the runs; therefore the values of k_6 represent a compromise between a high value needed to fit the large in-phase absorption at low frequency and a lower value needed to fit the data in the curve-crossing region. Thus the A_{τ_0} values for HO_2 in the O_2–N_2 system, calculated from the mean value of k_6 obtained from this data set, were significantly lower than those observed, as can be seen in Fig. 3. In contrast, the A_{τ_0} values estimated for $k_6 = 3.5 \times 10^{-11}$ cm^3 molecule^{-1} s^{-1} were higher than those observed and the corresponding low frequency absorptions were incompatible with the observed values unless a serious source of systematic error was present in these measurements. In the experiments using helium diluent a better fit to the observed A_{τ_0} values was obtained in the simulations but there was still a tendency to overestimate low frequency in-phase absorption in all cases.

The average value from all the data at 308 K is

$$k_6 = (6.2^{+4.0}_{-2.0}) \times 10^{-11} \text{ cm}^3 \text{ molecule}^{-1} \text{ s}^{-1}$$

The estimated overall error limits include both experimental error and possible systematic errors arising from the inability of the model to fit the detailed behaviour of HO_2 accurately. The larger uncertainty on the high side of the mean value reflects the requirement of a higher value of k_6 to fit the low frequency HO_2 data satisfactorily.

The mean value of σ_{OH} for absorption of the Q_{13} line and nearby features from the resonance lamp source was $(1.03 \pm 0.25) \times 10^{-16}$ cm^2 molecule^{-1}. This may be compared with a value of approximately 2×10^{-16}

TABLE 3

Rate coefficients for the reaction of OH with HO_2 obtained from computer simulations

$[O_3] \times 10^{-15}$ (molecules cm^{-3})	$[H_2O] \times 10^{-15}$ (molecules cm^{-3})	*Number of lamps*	$k_6 \times 10^{11}$ (cm^3 molecule^{-1} s^{-1})	$\sigma_{OH} \times 10^{17}$ (cm^2)	*Data fitted*
O_2–N_2 diluent at 308 K					
0.95	166	6	5.4 ± 0.4	—	HO_2
1.38	465	6	3.5 ± 0.4	—	HO_2
1.88	241	6	7.1 ± 1.0	—	HO_2
1.94	465	1	7.0 ± 0.7	—	HO_2
2.39	138	6	7.6 ± 0.9	—	HO_2
2.79	142	1	9.6 ± 0.7	—	HO_2
			6.8 ± 1.7 (mean value)		
2.39	138	6	$2.8^{+2.0}_{-1.0}$	0.76 ± 0.05	OH
Helium diluent at 308 K					
1.10		3	5.4 ± 0.5	—	HO_2
1.31	208	3	4.6 ± 0.4	—	HO_2
1.33	250	1	6.7 ± 0.6	—	HO_2
1.46	208	1	5.3 ± 0.6	1.11 ± 0.04	HO_2, OH
2.43	210	3	5.5 ± 0.6	1.04 ± 0.04	HO_2, OH
2.56	207	1	6.3 ± 0.3	—	HO_2
3.23	210	1	6.3 ± 0.5	1.02 ± 0.05	HO_2, OH
	207		5.7 ± 0.3 (mean value)		
0.43	209	3	$7.3^{+22.7}_{-5.6}$	1.24 ± 0.04	OH
O_2–N_2 diluent at 348 K					
0.79	443	6	$3.5^{+3.5}_{-1.8}$	—	HO_2
1.65	319	6	5.7 ± 0.8	—	HO_2
1.61	443	6	6.0 ± 1.0	—	HO_2
1.60	380	1	$11.0^{+3.0}_{-2.5}$	—	HO_2
O_2–N_2 diluent at 288 K					
1.69	512	6	4.4 ± 0.3	—	HO_2

cm^2 molecule^{-1}, which is obtained from the calculations of Smith and coworkers [20, 21] for a very similar experimental arrangement to that used in the present study but with total gas pressures of approximately 50 Torr in the reaction cell. Since the absorption lines are subject to collision broadening, a drop in the effective cross section can occur as the total gas pressure increases. A reduction by a factor of about 2 over the range 50 - 760 Torr is typical of that observed for OH absorption in flash photolysis–resonance absorption systems which have similar optical configurations to those used in the present work [22]; the present value of σ_{OH} is therefore entirely reasonable for the experimental conditions employed.

Table 3 also shows values of k_6 obtained from computer fits to the data obtained at 288 and 348 K. The mean value from the four experiments at 348 K was $k_6 = (6.5^{+4.5}_{-3.0}) \times 10^{-11}$ cm^3 molecule^{-1} s^{-1} and the single experi-

ment at 288 K gave $k_6 = (4.4 \pm 0.3) \times 10^{-11}$ cm^3 molecule^{-1} s^{-1}. The fit to the experimental data, as reflected in the sum of the squares of the residuals, was less good at 348 K than at 308 K but the fit to the 288 K data was excellent over the whole range of photolysis frequencies. It is concluded from these results that the average value of k_6 shows no significant temperature dependence over the rather limited temperature range investigated.

Simulations were performed to check the sensitivity of the optimized parameter k_6 to the values of the fixed parameters. The experimentally determined parameters k_a and $\Phi(-O_3)$ were considered to be accurate to within ±10%. A 10% decrease in k_a caused only a 5% decrease in k_6 whereas a similar change in $\Phi(-O_3)$ resulted in a 15% increase in k_6. This reflects the importance of accurately describing the modulation of O_3 over a photolysis cycle. The effect of k_3, k_4, k_5 and k_{11} on the optimized value of k_6 in selected data sets was checked by varying the rate coefficients within the uncertainty limits recommended in the CODATA evaluation [17]. The following results were obtained: $\Delta k_3 = +41\%$ gave $\Delta k_6 = +55\%$; $\Delta k_4 = -50\%$ gave $\Delta k_6 = -21\%$; $\Delta k_5 = +67\%$ gave $\Delta k_6 = -12\%$; $\Delta k_{11} = -50\%$ gave $\Delta k_6 = +10\%$. Clearly the parameter to which k_6 shows most sensitivity is k_3, but the error introduced from this source is considered to be unlikely to lead to a value of k_6 that is very far outside the error limits already stated.

Finally, the computed values for the functional plot of $\Phi(-O_3) - 1$ *versus* $[O_3]/B^{1/2}$ are compared with experimental data for a photolysis frequency of 1 Hz in Fig. 10. The trend in the data is well defined over the range. The computed data points using $k_6 = 3.5 \times 10^{-11}$ cm^3 molecule^{-1} s^{-1} generally overestimate the observed quantum yields, whereas with a value of k_6 of 1×10^{-10} cm^3 molecule^{-1} s^{-1} the predicted quantum yields are lower than those observed. Computations also predict a small increase in $\Phi(-O_3)$ with increasing photolysis frequencies, in accordance with observation.

4. Discussion

This computer analysis shows that the chemical model in Table 2 predicts satisfactorily the trends observed in the measured experimental parameters as functions of the radical production rate B and the O_3 concentration. This implies that the basic model for the photolysis of O_3–H_2O mixtures is correct inasmuch as the radicals are terminated mainly by a rapid reaction removing OH and HO_2 radicals simultaneously. However, the time dependence of the HO_2 absorption, which is the parameter showing greatest sensitivity to the rate of the OH + HO_2 reaction, is not accurately described throughout a photolysis cycle by a single value of k_6. This implies that either (a) there is a systematic error in the measurement of the HO_2 absorption or (b) the model for the behaviour of HO_2 is incomplete and/or the measured rate coefficient for the OH + HO_2 reaction in the present system is not simply that for the elementary bimolecular reaction step

$$OH + HO_2 \rightarrow H_2O + O_2 \qquad (6)$$

Measurements with our apparatus on systems with simple kinetics have exhibited model behaviour; thus systematic experimental errors of measurement are not a likely explanation. However, the presence of an additional transient species which absorbs at 210 nm could lead to a systematic error in monitoring HO_2 and this cannot be ruled out. Another possible source of systematic error in the determination of the behaviour of HO_2 could arise from inaccuracies in the description of $[O_3]$ modulation, which contributes markedly to the low frequency absorption components.

Before discussing possibility (b), it is of interest to consider previous measurements of k_6 which are listed in Table 4. Clearly the values measured at low pressure in discharge flow systems are lower than those obtained from both direct and steady state measurements at high pressure in systems which also all contained water vapour. These differences have been discussed in some detail by Howard [23] who has suggested that the overall reaction may proceed via two channels, namely a pressure-independent component in which OH abstracts the weakly bound hydrogen atom of HO_2 with a rate coefficient of 3×10^{-11} cm^3 molecule^{-1} s^{-1} and a pressure-dependent and possibly $[H_2O]$-dependent component which may proceed via an HO—OOH intermediate. The mean value of k_6 of 6.2×10^{-11} cm^3 molecule^{-1} s^{-1} obtained at 760 Torr pressure and 308 K in the present work is considerably lower than the other values obtained under similar conditions, implying that a simple pressure dependence cannot be invoked to explain the observations. However, our data are certainly not consistent with the lower values of k_6 obtained in discharge flow systems and we conclude that some kind of complex mechanism must be operative.

Several possible complex mechanisms involving polyoxides of hydrogen can be postulated for the OH + HO_2 reaction. Three polyoxides have been discussed recently in papers concerned with HO_x reactions. These are

TABLE 4

Measurements of the rate coefficient for the OH + HO_2 reaction at 300 K

k (cm^3 molecule^{-1} s^{-1})	*Total pressure* (Torr)	$[H_2O]$ (Torr)	*Method*[a]	*Reference*
$(5.1 \pm 1.6) \times 10^{-11}$	2 - 3	—	DF–LMR	7, 10
$(3 \pm 1) \times 10^{-11}$	2	—	DF–LMR	8
$(2 - 3) \times 10^{-11}$	2 - 4	—	DF–RF	9
1.6×10^{-10}	700	1 - 3	SS	4
$(1.2 \pm 0.25) \times 10^{-10}$	760	4.6	SS	5
$(1.16 \pm 0.25) \times 10^{-10}$	760	21	FP–absorption	12[b]
$(9.9 \pm 1.2) \times 10^{-11}$	1200	2 - 16	PR–absorption	13
$(6.2^{+4.0}_{-2.0}) \times 10^{-11}$	760	4 - 15	Molecular modulation	This work

[a] DF, discharge flow; LMR, laser magnetic resonance; RF, resonance fluorescence; SS, steady state photolysis; FP, flash photolysis; PR, pulse radiolysis.
[b] This result supersedes an earlier value of 2.0×10^{-10} cm^3 molecule^{-1} s^{-1} reported from the same laboratory [13].

$HO_2 \cdot H_2O$, the hydrate of the HO_2 radical [24, 25], H_2O_4, the dimer of HO_2 [16, 20, 26], and H_2O_3, which is formed in the association of OH with HO_2 [20, 27, 28]. These could be formed in the following gas phase processes:

$$HO_2 + H_2O \rightleftharpoons HO_2 \cdot H_2O \qquad \Delta H^\circ \approx -40 \text{ kJ mol}^{-1} \quad (16)$$

$$HO_2 + HO_2 \; (+ M) \rightleftharpoons H_2O_4 \; (+ M) \qquad \Delta H^\circ \approx -17 \text{ kJ mol}^{-1} \quad (17)$$

$$HO_2 + OH \; (+ M) \rightleftharpoons H_2O_3 \; (+ M) \qquad \Delta H^\circ \approx -117 \text{ kJ mol}^{-1} \quad (18)$$

Reaction of OH with any of these complexes by the general reaction

$$OH + H_xO_y \rightarrow H_2O + H_{x-1}O_y \qquad (19)$$

leads to the same net overall stoichiometry as reaction (6) does. If the equilibria (16) - (18) are maintained, the overall rate coefficient k_6' for the OH + HO_2 reaction takes the form

$$k_6' = k_6 + K_{19}C \qquad \text{(VII)}$$

where $C = K_{16}^*[H_2O]$, $K_{17}^*[HO_2]$ or $K_{18}^*[OH]$. This equation indicates that the overall rate coefficient could depend on the amounts of H_2O, HO_2 and OH present. If the equilibria are not maintained, *i.e.* if $k_{19}[OH] \geqslant k_{-16}$, k_{-17} or k_{-18}, the overall rate of the reaction of OH with HO_2 will depend on R_{16}, R_{17} and R_{18}. The resulting rate equation will exhibit a complex dependence on H_2O, HO_2, OH and total pressure. Although equilibrium can be safely assumed for the $HO_2 \cdot H_2O$ complex [25], it cannot be for H_2O_4 or H_2O_3. However, if a mechanism involving an equilibrated H_2O_3 species was occurring, the observed value of k_6' should be a marked function of [OH]. This is clearly not the case in the present system, since [OH] in the helium diluent experiments was 10 - 100 times greater than that in the O_2–N_2 diluent whereas the mean value of k_6' was unchanged. Furthermore, if $k_{19}[OH] \gg k_{-18}$ a simple pressure dependence of k_6' would result, which does not explain the difference between the present result and the other high pressure measurements. On this basis an important role for the H_2O_3 intermediate in the OH + HO_2 reaction does not seem likely but it cannot be entirely ruled out.

Involvement of the $HO_2 \cdot H_2O$ complex would be expected to lead to an $[H_2O]$ dependence of k_6'. It can be seen from Tables 3 and 4 that there is no evidence for a systematic increase in k(OH + HO_2) with $[H_2O]$, either in the present experimental values or in the other reported high pressure values. This suggests that the $HO_2 \cdot H_2O$ complex does not play a significant role in the kinetics of the reaction of OH with HO_2.

The formation of H_2O_4 is expected to be favoured by high pressure and high $[HO_2]$ and a mechanism involving this species would therefore appear to offer a potential explanation of the high values for k(OH + HO_2) measured under these conditions. This possibility was explored by further computer simulations of the present experimental results with reactions (17), (−17) and (19) included in the chemical scheme. An optimization calculation was carried out in which the values of k_{17} and k_{-17} were varied to fit the experi-

mental data shown in Fig. 2. k_6 was fixed at 3.5×10^{-11} cm^3 molecule^{-1} s^{-1} (the recommended value [17] based on the low pressure results) and k_{19} was fixed at 7.0×10^{-11} cm^3 molecule^{-1} s^{-1} (chosen on the basis of two equivalent hydrogen atoms present in H_2O_4). This fit gave

$$k_{17} = (1.6^{+1.6}_{-0.8}) \times 10^{-12} \text{ cm}^3 \text{ molecule}^{-1} \text{ s}^{-1}$$

$$k_{-17} \gtrsim 1 \text{ s}^{-1} \quad \text{(not well defined)}$$

but the corresponding computed curves for P and Q *versus* τ were almost identical with those obtained with the simple mechanism and with $k_6 = 7.6 \times 10^{-11}$ cm^3 molecule^{-1} s^{-1} (see Fig. 2). In other calculations various fixed combinations of k_{17} ($(2 - 20) \times 10^{-12}$ cm^3 molecule^{-1} s^{-1}), k_{-17} (1.0 - 100 s^{-1}) and k_{19} ($(7 - 30) \times 10^{-11}$ cm^3 molecule^{-1} s^{-1}), in the ranges indicated in parentheses, were used to predict the HO_2 absorption curves. Although it was found that the relative absorptions at τ_0 and $\tau \gg \tau_0$ (*i.e.* the shape of the curves) could be varied by different combinations of these rate coefficients, none of the combinations gave a really significant improvement in the fit to the experimental curves. It was concluded, however, that for H_2O_4 to play any significant role at all, the equilibrium constant K_{17}* needed to be greater than about 2×10^{-14} cm^3 molecule^{-1}. Since the rate coefficient for the association reaction (17) is unlikely to be greater than 4×10^{-11} cm^3 molecule^{-1} s^{-1} (*cf.* $k(CH_3 + CH_3 \rightarrow C_2H_6)$) this implies an upper limit of approximately 2×10^3 s^{-1} for the unimolecular dissociation rate constant k_{-17} at 308 K. This value of k_{-17} would require $D(HO_2 - O_2H) \geqslant 75$ kJ mol^{-1} (assuming $A_{-17} = 10^{16}$ s^{-1}) and therefore $\Delta H°(H_2O_4) \leqslant -56.5$ kJ mol^{-1} (this was computed using $\Delta H_f°(HO_2) = 10.5 \pm 2.1$ kJ mol^{-1} at 298 K [23]). This result is incompatible with the estimates of Nangia and Benson [28] which indicate a much lower stability for the linear polyoxide structure $\Delta H_f°(HOOOOH) \approx +4$ kJ mol^{-1}. Clearly more reliable information on the structure, thermochemistry and kinetics of H_2O_4 are required before its role in HO_x reactions in this and similar chemical systems can be ascertained.

In conclusion, the calculations we have performed show that the experimental data obtained in this study could be equally well described by a simple bimolecular reaction step for the OH + HO_2 reaction or by a complex mechanism of the type discussed, but the description in neither case was entirely satisfactory. If a complex mechanism is operative, as seems likely from the differences in the apparent values of k_6 determined in various experimental systems, elucidation of this mechanism is essential for a proper description of the behaviour of HO_2 and OH in the atmospheric environment. Clearly further experimental work will be necessary before this can be achieved.

Acknowledgments

This work is part of a programme of atmospheric pollution research sponsored jointly by the U.K. Department of the Environment and the European Economic Community Environmental Research Programme.

References

1 R. G. W. Norrish and R. P. Wayne, *Proc. R. Soc. London, Ser. A, 288* (1965) 200.
2 W. D. McGrath and R. G. W. Norrish, *Proc. R. Soc. London, Ser. A, 254* (1960) 317.
3 W. M. DeMore, *Science, 180* (1973) 735.
4 W. B. DeMore and E. Tschuikow-Roux, *J. Phys. Chem., 78* (1974) 1447.
5 W. B. DeMore, *J. Phys. Chem., 83* (1979) 1113.
6 G. Dixon-Lewis and D. J. Williams, Oxidation of hydrogen and carbon monoxide. In C. H. Bamford and C. F. H. Tipper (eds.), *Comprehensive Chemical Kinetics*, Vol. 17, Elsevier, Amsterdam, 1977.
7 J. P. Burrows, G. W. Harris and B. A. Thrush, *Nature (London), 267* (1977) 233.
8 W. Hack, A. W. Preuss and H. G. Wagner, *Ber. Bunsenges. Phys. Chem., 82* (1978) 1167.
9 J. S. Chang and F. Kaufman, *J. Phys. Chem., 82* (1978) 1683.
10 J. P. Burrows, D. I. Cliff, G. W. Harris, B. A. Thrush and J. P. T. Wilkinson, *Proc. R. Soc. London, Ser. A, 368* (1979) 463.
11 C. J. Hochanadel, J. A. Ghormley and P. J. Ogren, *J. Chem. Phys., 56* (1972) 4426.
12 C. J. Hochanadel, T. J. Sworski and P. J. Ogren, *J. Phys. Chem., 84* (1980) 3274.
13 R. R. Lii, R. A. Gorse, M. C. Sauer, Jr., and S. Gordon, *J. Phys. Chem., 84* (1980) 819.
14 R. A. Cox, R. G. Derwent, A. E. J. Eggleton and H. J. Reid, *J. Chem. Soc., Faraday Trans. I, 75* (1979) 1648.
15 M. Ackerman, in G. Fiocco (ed.), *Mesospheric Models and Related Experiments*, Reidel, Boston, 1971.
16 R. A. Cox and J. P. Burrows, *J. Phys. Chem., 83* (1979) 2560.
17 D. L. Baulch, R. A. Cox, R. F. Hampson, Jr., J. A. Kerr, J. Troe and R. T. Watson, *J. Phys. Chem. Ref. Data, 9* (1980) 295.
18 G. K. Moortgat, $O(^1D)$ quantum yields from O_3 photodissociation and $O(^1D)$ reactions with atmospheric constituents, *Proc. NATO Advanced Study Institute on Atmospheric Ozone, Aldeia das Acoteias, October 1 - 13, 1979*, p. 599; *Rep. FAA-EE-80-20* (U.S. Department of Transportation).
19 E. M. Chance, A. R. Curtis and C. R. Kirby, FACSIMILE: a computer program for flow and chemistry simulation and general initial value problems, *AERE Rep. R 8775*, Her Majesty's Stationery Office, London, 1977.
20 I. W. M. Smith and R. Zellner, *J. Chem. Soc., Faraday Trans. II, 69* (1973) 1617.
21 C. Anastasi and I. W. M. Smith, *J. Chem. Soc., Faraday Trans. II, 72* (1976) 1459.
22 I. W. M. Smith, personal communication.
23 C. J. Howard, Laboratory studies of reactions of odd hydrogen species of atmospheric interest, *Proc. NATO Advanced Study Institute on Atmospheric Ozone, Aldeia das Acoteias, October 1 - 13, 1979*, p. 409; *Rep. FAA-EE-80-30* (U.S. Department of Transportation).
24 E. J. Hamilton, Jr., *J. Chem. Phys., 63* (1975) 3682.
25 E. J. Hamilton and R. R. Lii, *Int. J. Chem. Kinet., 9* (1977) 875.
26 B. A. Thrush and J. P. T. Wilkinson, *Chem. Phys. Lett., 66* (1979) 441.
27 P. A. Giguere and K. Herman, *Can. J. Chem., 48* (1970) 3473.
28 P. S. Nangia and S. W. Benson, *J. Phys. Chem., 83* (1979) 1138.